

# Nanoscale synthesis and affinity ranking

Nathan J. Gesmundo<sup>1,3</sup>, Bérengère Sauvagnat<sup>2</sup>, Patrick J. Curran<sup>2</sup>, Matthew P. Richards<sup>2</sup>, Christine L. Andrews<sup>2</sup>, Peter J. Dandliker<sup>2</sup> & Tim Cernak<sup>1,4\*</sup>

Most drugs are developed through iterative rounds of chemical synthesis and biochemical testing to optimize the affinity of a particular compound for a protein target of therapeutic interest. This process is challenging because candidate molecules must be selected from a chemical space of more than  $10^{60}$  drug-like possibilities<sup>1</sup>, and a single reaction used to synthesize each molecule has more than  $10^7$  plausible permutations of catalysts, ligands, additives and other parameters<sup>2</sup>. The merger of a method for high-throughput chemical synthesis with a biochemical assay would facilitate the exploration of this enormous search space and streamline the hunt for new drugs and chemical probes. Miniaturized high-throughput chemical synthesis<sup>3–7</sup> has enabled rapid evaluation of reaction space, but so far the merger of such syntheses with bioassays has been achieved with only low-density reaction arrays, which analyse only a handful of analogues prepared under a single reaction condition<sup>8–13</sup>. High-density chemical synthesis approaches that have been coupled to bioassays, including on-bead<sup>14</sup>, on-surface<sup>15</sup>, on-DNA<sup>16</sup> and mass-encoding technologies<sup>17</sup>, greatly reduce material requirements, but they require the covalent linkage of substrates to a potentially reactive support, must be performed under high dilution and must operate in a mixture format. These reaction attributes limit the application of transition-metal catalysts, which are easily poisoned by the many functional groups present in a complex mixture, and of transformations for which the kinetics require a high concentration of reactant. Here we couple high-throughput nanomole-scale synthesis with a label-free affinity-selection mass spectrometry bioassay. Each reaction is performed at a 0.1-molar concentration in a discrete well to enable transition-metal catalysis while consuming less than 0.05 milligrams of substrate per reaction. The affinity-selection mass spectrometry bioassay is then used to rank the affinity of the reaction products to target proteins, removing the need for time-intensive reaction purification. This method enables the primary synthesis and testing steps that are critical to the invention of protein inhibitors to be performed rapidly and with minimal consumption of starting materials.

The merger of nanoscale synthesis with affinity ranking, which we call NanoSAR, could enable data-rich interrogations of reaction–chemical–bioactivity space (Fig. 1). Nanoscale synthesis consumes less than 0.05 mg of substrate per reaction<sup>3</sup>, so precious starting materials such as complex drug-like intermediates can be used. Affinity-selection mass spectrometry (ASMS) is a sensitive bioassay<sup>18,19</sup> that relates protein binding to mass detection of a candidate molecule. ASMS was chosen to assay crude nanoscale reaction mixtures directly because misleading readouts related to catalysts or other reaction components can be omitted as long as the molecular masses of the desired products and residual reagents can be resolved by high-resolution mass spectrometry. However, most existing ASMS protocols provide only a binary readout of affinity<sup>20</sup>. We envisioned that affinity could be ranked by titrating down the concentration of protein while maintaining a constant concentration of compound. As the protein concentration decreases, competition for binding is induced<sup>21</sup>, and only compounds with high affinity to the target are observed at the lowest

protein concentration. With this advance, potent protein inhibitors may be identified at a nanomole-scale while forgoing time-consuming reaction purification.

We validated NanoSAR by synthesizing libraries based on three of the most popular transformations used in pharmaceutical research<sup>22,23</sup>. Each library contains about 20 compounds and each reaction was run on a nanomole scale (less than 0.05 mg). Every analogue was resynthesized on a traditional scale (about 20 mg) so that bioassay results of unpurified nanoscale reactions could be compared directly to data obtained from purified products using a conventional approach. The crude nanoscale reaction mixtures were analysed by using ultra-high-performance liquid chromatography–mass spectrometry (UPLC–MS) to evaluate the reaction efficiency, pooled, and submitted to the ASMS affinity-ranking assay directly (Extended Data Fig. 1). Next, each product was resynthesized on an approximately 20-mg scale using the productive reaction conditions identified on the nanoscale and purified. These purified products were likewise submitted to the ASMS affinity-ranking assay, but were also either submitted to a traditional assay of biochemical function or compared to reported binding affinities. Potent molecules could be identified regardless of the scale of the reaction.

The bioassay results from the crude nanoscale reactions matched those obtained from the purified products. For example, a library of 19 known inhibitors<sup>24</sup> of the kinase ERK2 was prepared by allowing carboxylic acid **1** to react with diverse amines in the presence of HATU (hexafluorophosphate azabenzotriazole tetramethyl uronium) and <sup>i</sup>Pr<sub>2</sub>NEt (19 reactions, Fig. 2a) and submitted to affinity ranking. High-affinity amide product **2** (inhibitory constant  $K_i = 35$  nM), which was

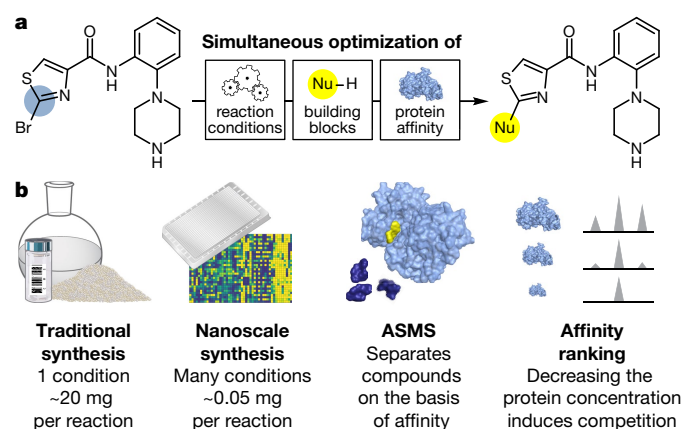


**Fig. 1 | Nanoscale synthesis and affinity ranking (NanoSAR).**

**a**, Reaction space and chemical space are navigated at the nanomole-scale and bioassayed directly to locate potent protein inhibitors and productive reaction conditions simultaneously. **b**, Nanoscale synthesis consumes a fraction of the material that is required for traditional synthesis. Crude reactions are assayed by ASMS, with affinity ranking achieved by decreasing the concentration of the target protein to induce competition among compounds.

<sup>1</sup>Department of Discovery Chemistry, Merck & Co., Inc., Boston, MA, USA. <sup>2</sup>Department of Pharmacology, Merck & Co., Inc., Boston, MA, USA. <sup>3</sup>Present address: Research and Development, AbbVie, North Chicago, IL, USA. <sup>4</sup>Present address: Department of Medicinal Chemistry, Department of Chemistry, Program in Chemical Biology, University of Michigan, Ann Arbor, MI, USA. \*e-mail: tcernak@umich.edu

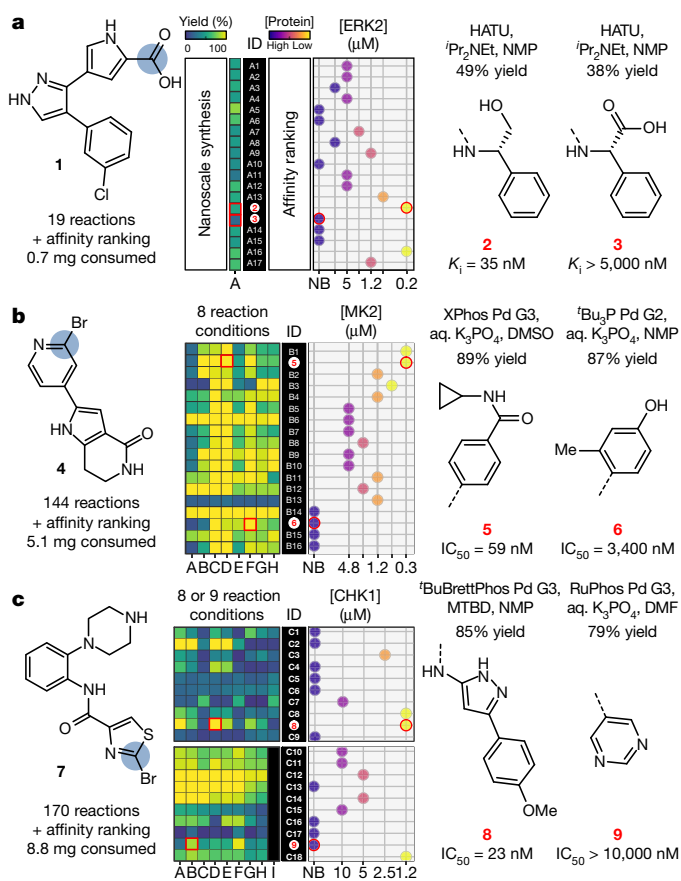


**Fig. 2 | NanoSAR identification of ERK2, MK2 and CHK1 inhibitors.** Inhibitors were produced using nanoscale synthesis and submitted directly to an ASMS affinity-ranking assay, then resynthesized on a 50- $\mu$ mol scale, purified, and reassayed by ASMS for comparison to the functional bioactivity ( $IC_{50}$ ) or reported binding affinity ( $K_i$ ) of each compound. **a**, A library of 19 ERK2 inhibitors prepared by amide coupling. **b**, A library of 18 MK2 inhibitors prepared by Suzuki coupling. **c**, A library of 20 CHK1 inhibitors prepared by Suzuki and C–N coupling. In each library, every compound has a unique identifier (ID) and was formed under one or more reaction conditions, with the yield, determined by UPLC, for each reaction depicted in the heat map and the affinity-ranking data depicted in the scatter plot. One high-affinity compound (2, 5 and 8) and one low-affinity compound (3, 6 and 9) from each library are shown. The reaction conditions identified on the nanoscale (red box) were then used for the 50- $\mu$ mol-scale resynthesis of each exemplary compound, and the corresponding affinity-ranking data for that compound are highlighted (red circle). NB indicates no binding was observed in the affinity-ranking assay at the highest protein concentration tested. See Extended Data Figs. 2–4 for reaction conditions (A–I), structures, yields and  $K_i$  or  $IC_{50}$  values of all compounds.

observed at the lowest ERK2 concentration tested in the affinity-ranking assay, was easily distinguished from low-affinity amide product 3 ( $K_i > 5,000$  nM), which was not observed at any of the ERK2 concentrations tested. Therefore, with NanoSAR it was possible to differentiate potent from impotent analogues with less than 0.05 mg of material and with no reaction purification (Extended Data Fig. 2).

For this library of ERK2 inhibitors produced by amide coupling, a single reaction condition was sufficient. For subsequent transition-metal-catalysed Suzuki or C–N coupling reactions, we surveyed eight and nine reaction conditions, respectively, to ensure that every product was synthesized successfully. Nanoscale Suzuki coupling of heterocyclic bromide 4 with 18 diverse boronates was achieved with 8 combinations of Buchwald precatalysts<sup>25</sup>, bases and solvents (144 reactions, Fig. 2b). Using conditions identified at the nanoscale, all 18 products were prepared on a traditional 50- $\mu$ mol scale,

purified and assayed for inhibition of the function of the kinase MK2<sup>26</sup>. NanoSAR can readily distinguish potent inhibitors, such as 5 (half-maximal inhibitory concentration  $IC_{50} = 59$  nM), from impotent inhibitors, such as 6 ( $IC_{50}$  3,400 nM).  $IC_{50}$  values for all 18 analogues were determined, using purified compounds produced on a 50- $\mu$ mol scale, and could be predicted from the NanoSAR data (Extended Data Fig. 3). Similarly, bromide 7 was used to generate 20 distinct inhibitors<sup>27</sup> of the kinase CHK1 via C–C and C–N coupling (170 reactions, Fig. 2c). Potent inhibitors, such as 8 ( $IC_{50}$  23 nM), were readily distinguished from an array of less-potent, lower-affinity compounds, such as 9 ( $IC_{50} > 10,000$  nM). Once again, affinity-ranking results from crude nanoscale reactions predicted the CHK1 functional activity of purified samples produced on a micromole scale (Extended Data Fig. 4). Samples treated with a metal scavenging resin had low levels of residual palladium; however, simple dilution with water reduced palladium levels to less than 5 p.p.m. (Extended Data Fig. 5).

The information density produced by NanoSAR permits explorations that were previously impractical or impossible, such as the rapid survey of reaction conditions, building blocks and protein affinity (Fig. 3). For example, 7 was coupled to various functionalized nucleophiles via multiple distinct chemical transformations, with affinity information for CHK1 generated for each analogue of the form of 10 produced. As shown in the outer reaction-condition heat map in Fig. 3, we explored combinations of catalysts (11–26), bases (27–34) and solvents (*N*-methyl pyrrolidinone (NMP), dimethylsulfoxide (DMSO) and *N,N*-dimethylformamide (DMF)) with 17 representative nucleophiles (D1–D17, Extended Data Fig. 6). For each class of nucleophile, four of the most productive reaction conditions were selected so that 7 could be effectively coupled to 384 diverse building blocks, as shown in the inner heat map of building-block reactivity (Fig. 3). By using four reaction conditions, we identified productive C–N, C–O, C–S or C–C coupling conditions for 345 of 384 products (90%) (Extended Data Figs. 7, 10). The 345 crude reaction mixtures, outlined in black in the inner heat map, were submitted directly to affinity ranking by titrating the CHK1 concentration from 10  $\mu$ M to 0.2  $\mu$ M: products that bind tightly to CHK1 appear closer to the centre of the circle in the affinity-ranking plot (Fig. 3). Key compounds were identified for scale-up, purification and analysis in an assay of CHK1 functional activity (Extended Data Fig. 8). Exemplars (35–41) are shown in Fig. 3 (see Extended Data Fig. 9 for dose titration curves), with each class of functional group revealing unique structure–reactivity and structure–bioactivity relationships. Compounds 38, 39 and 41 were isolated in 98%, 52% and 24% yield, respectively, from reactions run on a 50- $\mu$ mol scale, and were potent CHK1 inhibitors, as predicted by NanoSAR.

Subtle reactivity trends were illuminated in the data analysis. For instance, one of the thiol nucleophiles that we tested in the initial survey of reaction conditions (3-phenylpropane-1-thiol, D15) couples to 7 in high yield regardless of the catalyst, base or solvent used (see Extended Data Fig. 6 for reaction-condition mapping). This finding suggests that alkyl thiols couple to 7 via a nucleophilic aromatic substitution ( $S_NAr$ ) mechanism rather than via palladium catalysis. Guided by this information, two of the four reaction conditions selected to couple thiols to 7 used no catalyst. Compound 35 was isolated in 98% yield on a 50- $\mu$ mol scale using no catalyst, with  $P_2Et$  in DMF; however, it was inactive against CHK1, as predicted by NanoSAR.

Higher-order trends also emerge from the data. For example, comparing the reaction performance of boronate to amine building blocks suggests that, at least with 7, the Suzuki coupling is a more robust reaction than is the C–N coupling. Years of anecdotal experience with these two transformations led us to hypothesize this disparity in reaction robustness<sup>7</sup>, and here the phenomenon can be readily visualized. Patterns of bioactivity are also apparent in the central plot of affinity ranking in Fig. 3. For instance, many of the boronate-, amide- and amine-derived products were bioactive, exhibiting affinity to CHK1 and appearing as points closer to the centre of the circle; these compounds exhibited functional inhibition of CHK1 function



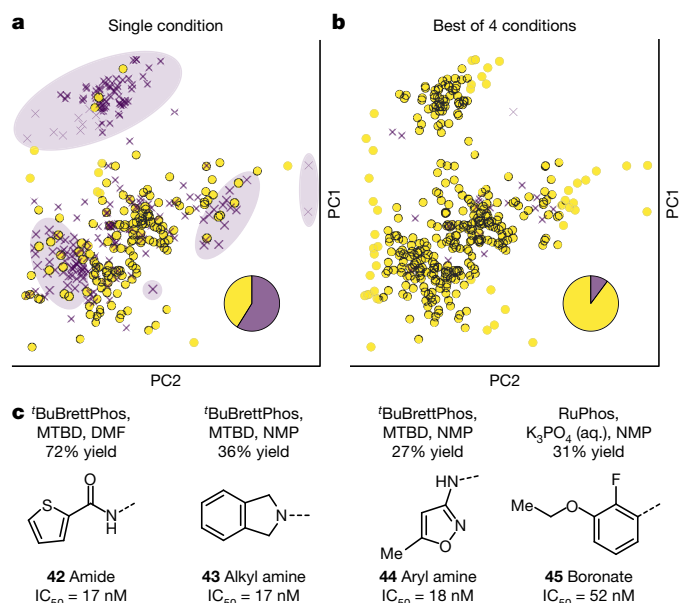


**Fig. 4 | NanoSAR enhances coverage of chemical space.** **a**, When coupling **7** to diverse nucleophiles (**D18–D402**), a single reaction condition (**11**, **27**, NMP, room temperature) produced 158 (yellow circles) out of 384 (41%; see inset pie chart) designed products, with 226 failures (0% yield; purple crosses). The purple highlighted regions indicate ‘dark’ regions of principal component (PC) chemical space, where reactions failed. **b**, Matching each nucleophile to the best of four reaction conditions produced 345 out of 384 (90%) products. **c**, 21 compounds from the ‘dark’ space that were made accessible by NanoSAR bound to CHK1, such as **42–45**. CHK1 IC<sub>50</sub> values are from a functional assay of purified compounds.

(Extended Data Fig. 9). By contrast, few of the sulfonamide-, thiol-, alkyne- or alcohol-derived products bound to CHK1, and these linkages could reasonably be deprioritized from future design cycles. In total, only 123 mg of **7** were consumed to run 3,114 reactions, to match 345 of the 384 diverse nucleophiles with coupling conditions, to assay the products and to paint a landscape of reactivity and bioactivity.

For comparison, coupling of bromide **7** to the same 384 diverse nucleophiles under a single reaction condition—the recently reported combination of <sup>t</sup>BuXPhos Pd G3 (**11**)<sup>25</sup> with P<sub>2</sub>Et (**27**) as a base<sup>28</sup>, which is among the most substrate-tolerant palladium-catalysed coupling conditions known<sup>7</sup>—yielded detectable product (**10**) for only 158 of 384 reactions (41%). Therefore, screening reaction conditions by using nanoscale synthesis enabled deeper exploration of chemical space, with an additional 187 targeted compounds synthesized and assayed successfully (Fig. 4). Under a single reaction condition, synthesis was unsuccessful for large swaths of chemical space and for compounds on the fringes of the space that we studied (Fig. 4a). NanoSAR identified 21 compounds from this ‘dark’ space that bound to CHK1 (Extended Data Fig. 10). Exemplary compounds were resynthesized at a 50- $\mu$ mol scale, purified and tested in a functional assay, whereupon several products (such as **42–45**) displayed functional inhibition of CHK1 at low, nanomolar concentrations (Fig. 4c). As can be seen from Fig. 3, a large number of reactions produce no observable product and a large number of compounds have no affinity to the protein target, which, in our experience, is typical of drug discovery. Machine-learning algorithms may one day facilitate the navigation of these problems<sup>29,30</sup>; however, locating bioactive molecules and conditions for their synthesis for now remains an experimental science, which NanoSAR is well positioned to accelerate.

### Data availability

The data that support the findings of this study are available within the paper and its Supplementary Information. Source Data for Figs. 2–4 and Extended Data Figs. 2–6, 8–10 are available with the online version of the paper.

### Online content

Any Methods, including any statements of data availability and Nature Research reporting summaries, along with any additional references and Source Data files, are available in the online version of the paper at <https://doi.org/10.1038/s41586-018-0056-8>.

Received: 2 October 2017; Accepted: 14 February 2018;

Published online: 23 April 2018

- Reymond, J. L. The chemical space project. *Acc. Chem. Res.* **48**, 722–730 (2015).
- Murray, P. M., Tyler, S. N. G. & Moseley, J. D. Beyond the numbers: charting chemical reaction space. *Org. Process Res. Dev.* **17**, 40–46 (2013).
- Buitrago Santanilla, A. et al. Nanomole-scale high-throughput chemistry for the synthesis of complex molecules. *Science* **347**, 49–53 (2015).
- Shevlin, M. Practical high-throughput experimentation for chemists. *ACS Med. Chem. Lett.* **8**, 601–607 (2017).
- Collins, K. D., Gensch, T. & Glorius, F. Contemporary screening approaches to reaction discovery and development. *Nat. Chem.* **6**, 859–871 (2014).
- Troshin, K. & Hartwig, J. F. Snap deconvolution: an informatics approach to high-throughput discovery of catalytic reactions. *Science* **357**, 175–181 (2017).
- Kutchukian, P. S. et al. Chemistry informer libraries: a cheminformatics enabled approach to evaluate and advance synthetic methods. *Chem. Sci.* **7**, 2604–2613 (2016).
- Werner, M. et al. Seamless integration of dose-response screening and flow chemistry: efficient generation of structure–activity relationship data of  $\beta$ -secretase (BACE1) inhibitors. *Angew. Chem. Int. Ed.* **53**, 1704–1708 (2014).
- Desai, B. et al. Rapid discovery of a novel series of Abl kinase inhibitors by application of an integrated microfluidic synthesis and screening platform. *J. Med. Chem.* **56**, 3033–3047 (2013).
- Guetzoyan, L., Nikbin, N., Baxendale, I. R. & Ley, S. V. Flow chemistry synthesis of zolpidem, alpidem and other GABA agonists and their biological evaluation through the use of in-line frontal affinity chromatography. *Chem. Sci.* **4**, 764–769 (2013).
- Karageorgis, G., Dow, M., Aimon, A., Warriner, S. & Nelson, A. Activity-directed synthesis with intermolecular reactions: development of a fragment into a range of androgen receptor agonists. *Angew. Chem. Int. Ed.* **54**, 13538–13544 (2015).
- Murray, J. B., Roughley, S. D., Matassova, N. & Brough, P. A. Off-rate screening (ORS) by surface plasmon resonance. An efficient method to kinetically sample hit to lead chemical space from unpurified reaction products. *J. Med. Chem.* **57**, 2845–2850 (2014).
- Baranczak, A. et al. Integrated platform for expedited synthesis–purification–testing of small molecule libraries. *ACS Med. Chem. Lett.* **8**, 461–465 (2017).
- Price, A. K., MacConnell, A. B. & Paegel, B. M. huSABR: photochemical dose–response bead screening in droplets. *Anal. Chem.* **88**, 2904–2911 (2016).
- Vastl, J., Wang, T., Trinh, T. B. & Spiegel, D. A. Encoded silicon-chip-based platform for combinatorial synthesis and screening. *ACS Comb. Sci.* **19**, 255–261 (2017).
- Goodnow, R. A. Jr, Dumelin, C. E. & Keefe, A. D. DNA-encoded chemistry: enabling the deeper sampling of chemical space. *Nat. Rev. Drug Discov.* **16**, 131–147 (2017).
- Annis, D. A. et al. An affinity selection–mass spectrometry method for the identification of small molecule ligands from self-encoded combinatorial libraries. Discovery of a novel antagonist of *E. coli* dihydrofolate reductase. *Int. J. Mass Spectrom.* **238**, 77–83 (2004).
- Andrews, C. L., Ziebell, M. R., Nickbarg, E. & Yang, X. in *Protein and Peptide Mass Spectrometry in Drug Discovery* (eds Gross, M. L. et al.) 253–286 (John Wiley & Sons, Hoboken, 2012).
- O’Connell, T. N., Ramsay, J., Rieth, S. F., Shapiro, M. J. & Stroh, J. G. Solution-based indirect affinity selection mass spectrometry—a general tool for high-throughput screening of pharmaceutical compound libraries. *Anal. Chem.* **86**, 7413–7420 (2014).
- Annis, D. A. et al. A general technique to rank protein–ligand binding affinities and determine allosteric versus direct binding site competition in compound mixtures. *J. Am. Chem. Soc.* **126**, 15495–15503 (2004).
- Cuozzo, J. W. et al. Discovery of a potent BTK inhibitor with a novel binding mode by using parallel selections with a DNA-encoded chemical library. *ChemBioChem* **18**, 864–871 (2017).
- Schneider, M. et al. Big data from pharmaceutical patents: a computational analysis of medicinal chemists’ bread and butter. *J. Med. Chem.* **59**, 4385–4402 (2016).
- Brown, D. G. & Boström, J. Analysis of past and present synthetic methodologies on medicinal chemistry: where have all the new reactions gone? *J. Med. Chem.* **59**, 4443–4458 (2016).
- Aronov, A. M. et al. Flipped out: structure-guided design of selective pyrazolopyrrole ERK inhibitors. *J. Med. Chem.* **50**, 1280–1287 (2007).
- Bruno, N. C., Tudge, M. T. & Buchwald, S. L. Design and preparation of new palladium precatalysts for C–C and C–N cross-coupling reactions. *Chem. Sci.* **4**, 916–920 (2013).
- Anderson, D. R. et al. Pyrrolopyridine inhibitors of mitogen-activated protein kinase-activated protein kinase 2 (MK-2). *J. Med. Chem.* **50**, 2647–2654 (2007).
- Huang, X. et al. Structure-based design and optimization of 2-aminothiazole-4-carboxamide as a new class of CHK1 inhibitors. *Bioorg. Med. Chem. Lett.* **23**, 2590–2594 (2013).

28. Buitrago Santanilla, A. et al. P<sub>2</sub>Et phosphazene: a mild, functional group tolerant base for soluble, room temperature Pd-catalyzed C–N, C–O, and C–C cross-coupling reactions. *Org. Lett.* **17**, 3370–3373 (2015).
29. Schneider, P. & Schneider, G. De novo design at the edge of chaos. *J. Med. Chem.* **59**, 4077–4086 (2016).
30. Ahneman, D. T., Estrada, J. G., Lin, S., Dreher, S. D. & Doyle, A. G. Predicting reaction performance in C–N cross coupling using machine learning. *Science* **360**, 186–190 (2018).

**Acknowledgements** We are grateful to L. Nogle, D. Smith and M. Pietrafitta (MSD) for assistance with compound purification, S. Bano and X. Bu (MSD) for measuring residual palladium concentrations, A. M. Norris (MSD) for assistance with graphics and Z. Gu (DFKZ German Cancer Research Center) for suggestions for data visualization. N.J.G. was supported by an MRL Postdoctoral Research Fellowship.

**Reviewer information** *Nature* thanks J. Janey, D. Young and the other anonymous reviewer(s) for their contribution to the peer review of this work.

**Author contributions** N.J.G., P.J.D. and T.C. conceived the study and wrote the manuscript. N.J.G., B.S., P.J.C., P.J.D. and T. C. designed and executed the experiments and analysed the data. C.L.A. and M.P.R. developed the protein titration method. T.C. supervised the work.

**Competing interests** The authors declare no competing interests.

**Additional information**

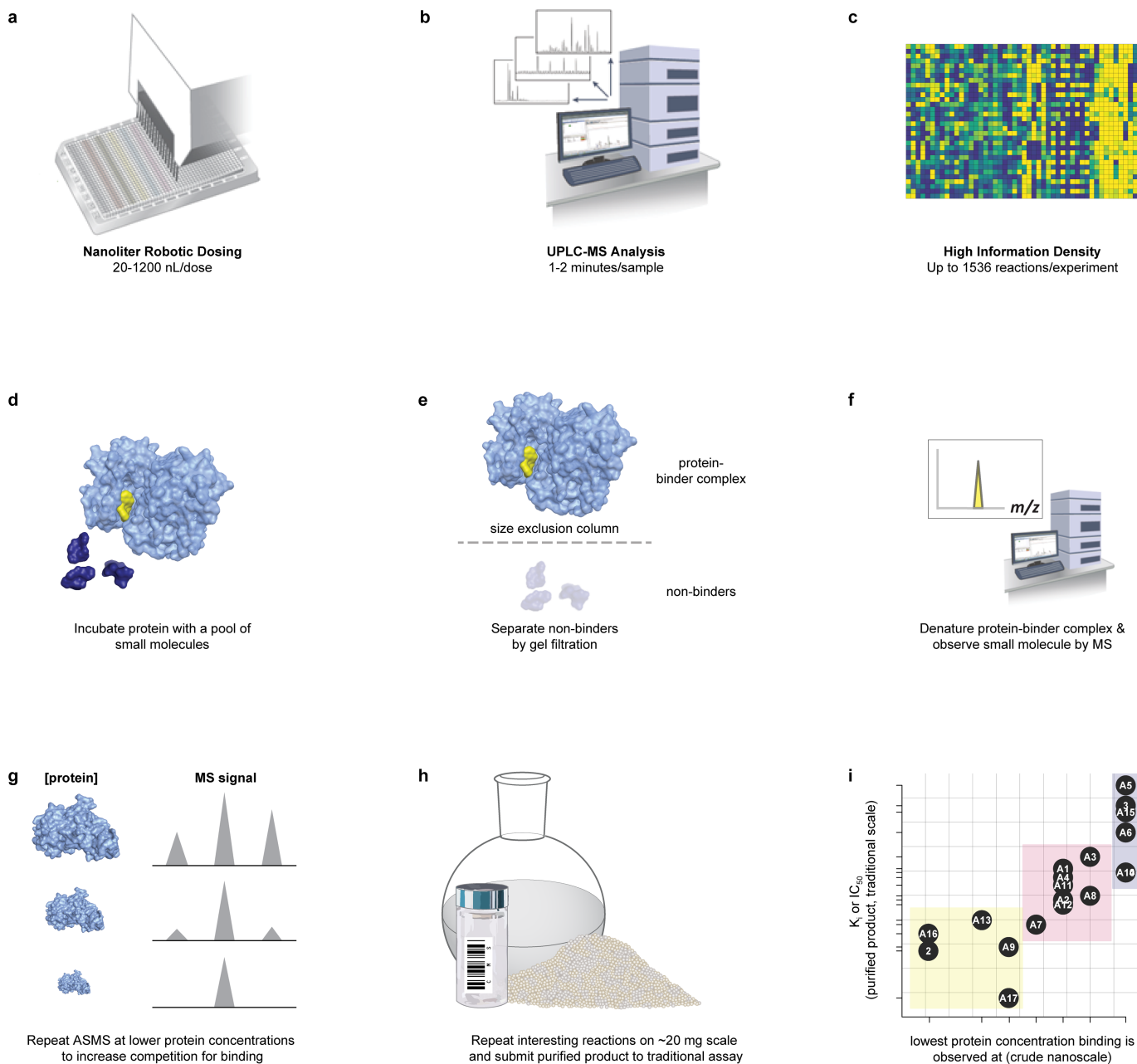
**Extended data** is available for this paper at <https://doi.org/10.1038/s41586-018-0056-8>.

**Supplementary information** is available for this paper at <https://doi.org/10.1038/s41586-018-0056-8>.

**Reprints and permissions information** is available at <http://www.nature.com/reprints>.

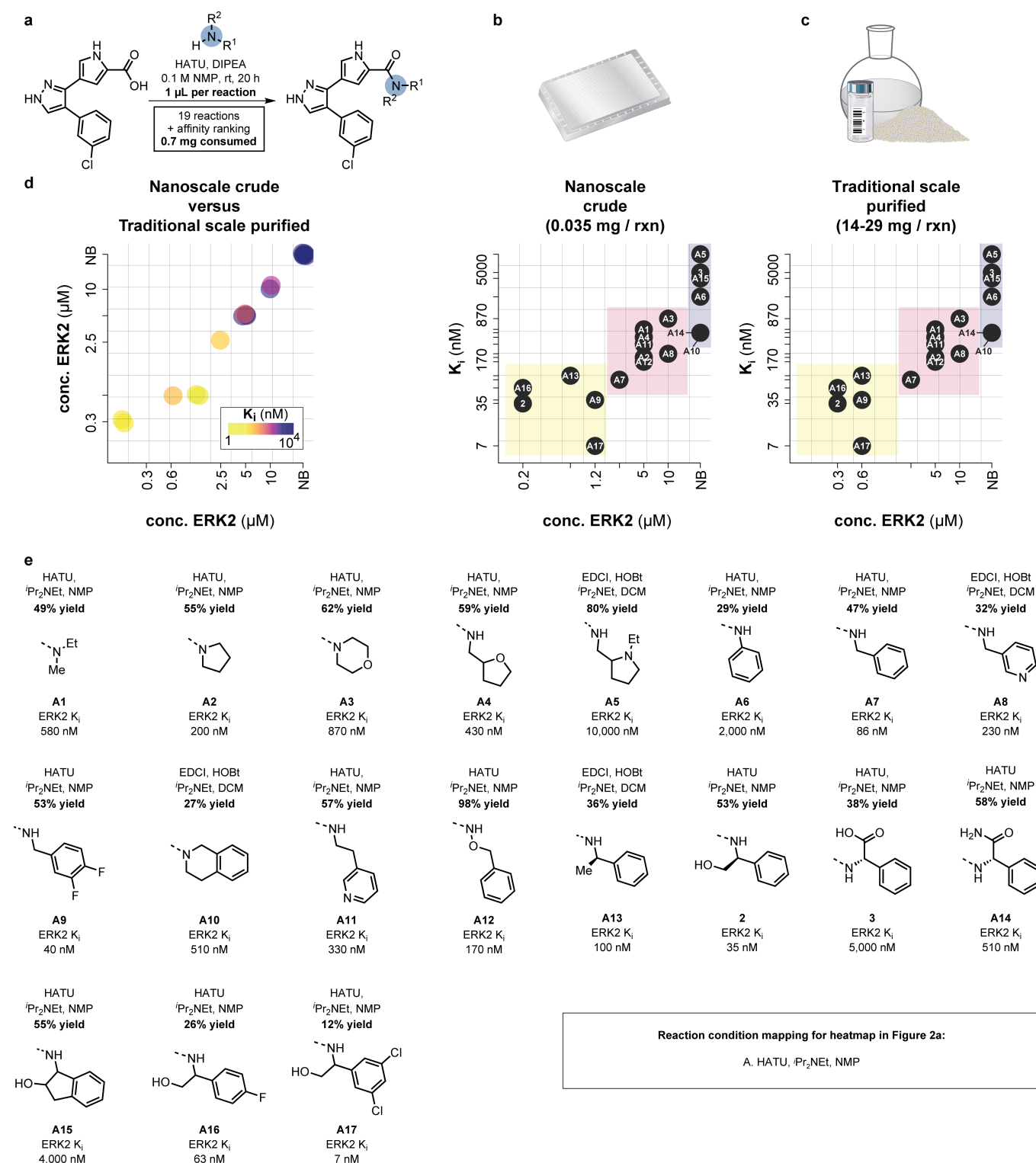
**Correspondence and requests for materials** should be addressed to T.C.

**Publisher's note:** Springer Nature remains neutral with regard to jurisdictional claims in published maps and institutional affiliations.



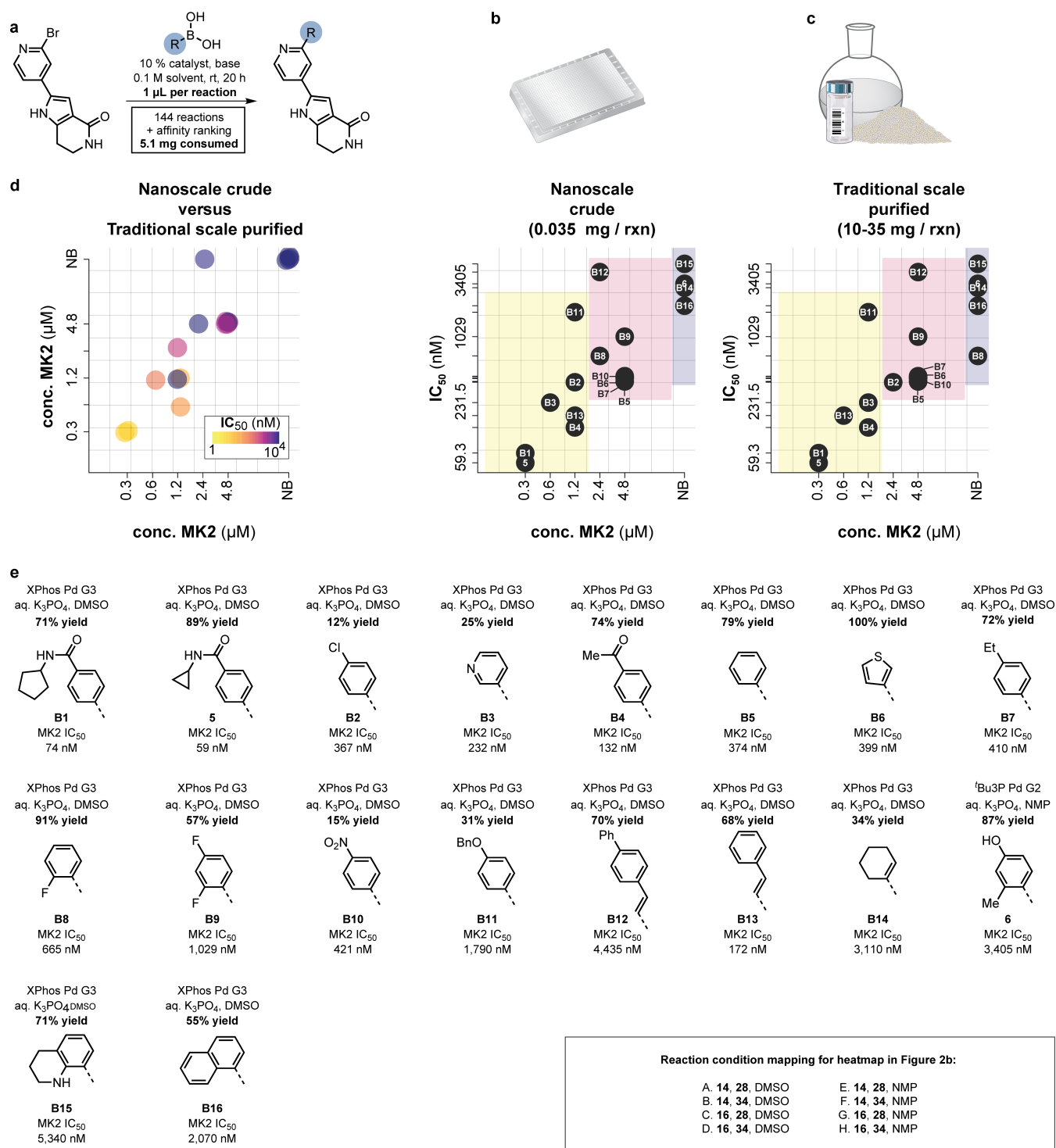
**Extended Data Fig. 1 | Additional details of the nanoscale synthesis and affinity ranking workflow.** **a**, Reaction solutions are dosed using a TTP mosquito liquid-handling robot that handles increments of 20 nl. **b**, c, UPLC-MS analysis confirms the presence of products from crude reactions (**b**), which is visualized in heat maps (**c**). **d**, For the ASMS assay, productive reactions are mass-encoded, pooled and incubated with a protein of interest. **e**, **f**, Elution through a size-exclusion column separates protein-bound compounds from unbound compounds (**e**), and binders

can be observed by high-performance liquid chromatography-mass spectrometry (HPLC-MS) following denaturation of the protein-ligand complex (**f**). **g**, Decreasing the concentration of protein in the ASMS assay increases the competition for binding so that ligands can be categorized as high, medium or low affinity. **h**, Scale-up of compounds and purification by using a traditional approach. **i**, Measurement of  $IC_{50}$  in a functional assay enables comparison of the new method to existing assay technology. See Supplementary Information for additional details.



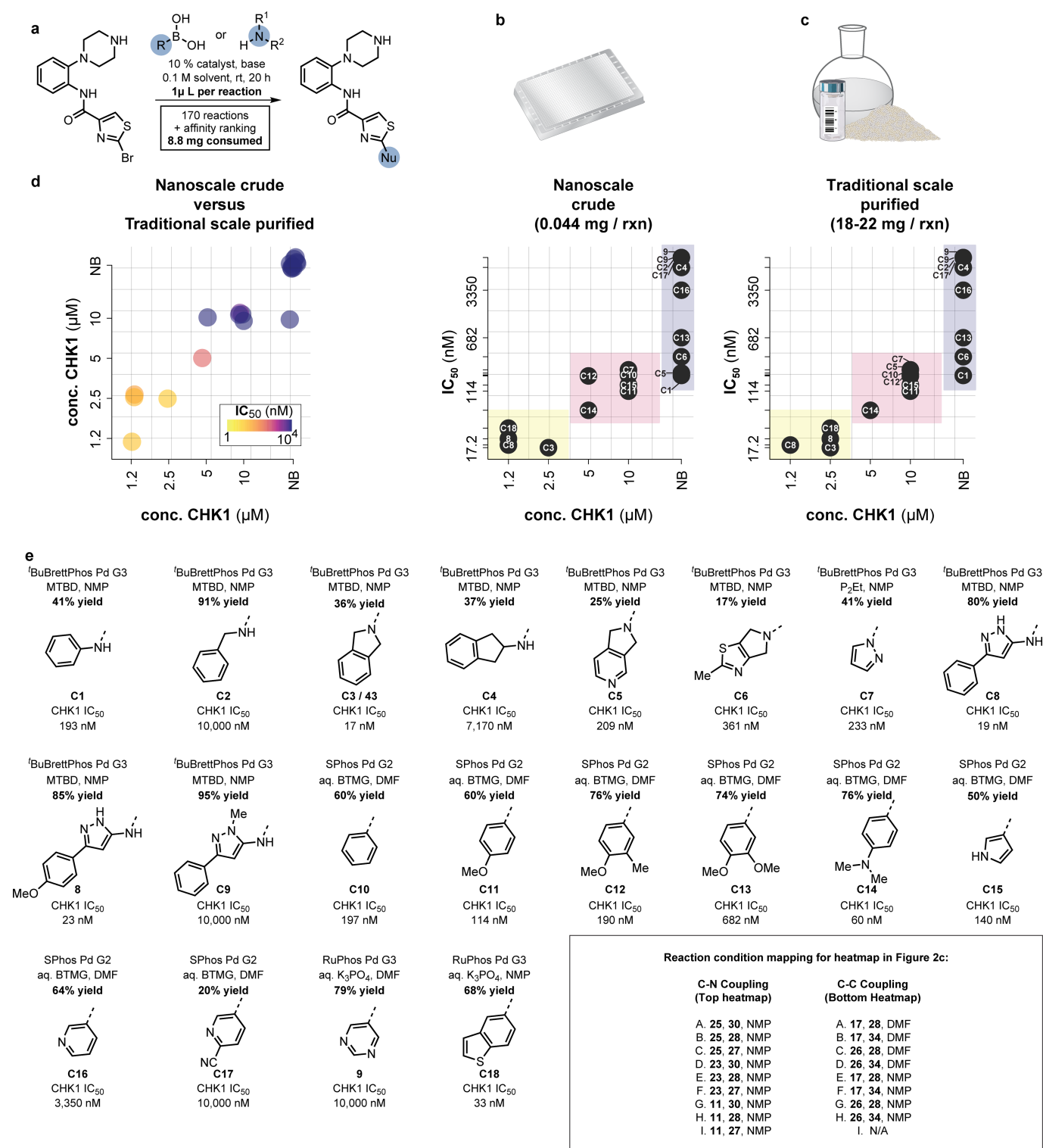
**Extended Data Fig. 2 | Structures, yields,  $K_i$  values and ASMS comparison plots for the ERK2 library.** **a**, A library of 19 unique ERK2 inhibitors (**2**, **3**, **A1**–**A17**) was produced by coupling **1** to diverse amines under a single reaction condition (HATU,  $i$ Pr<sub>2</sub>NEt, NMP; see Fig. 2a). **b**, Crude nanoscale reactions were submitted to the ASMS assay, with affinity ranking determined by reducing the concentration of ERK2 to increase the competition for binding. The lowest ERK2 concentration at which the mass signal of the compound was still observed is shown on the abscissa. The  $K_i$  value reported<sup>24</sup> from purified product samples generated on a 500-times-larger reaction scale is shown on the ordinate. The colour shading groups compounds into low affinity (purple), modest

affinity (magenta) or high affinity (yellow), as determined by the ASMS assay. rxn. reaction. **c**, Comparison of the results of the ASMS affinity-ranking assay (abscissa) to the reported ERK2  $K_i$  values (ordinate). Both datasets are from purified product samples produced on a 50- $\mu$ mol scale. **d**, Comparison of results of ASMS affinity ranking from crude reaction mixtures generated on a 100-nmol scale with those from purified product samples generated on a 50- $\mu$ mol scale. Points are coloured by  $K_i$ , and jittering was applied to this categorical data to reveal overlapping data. **e**, Product structures with reaction conditions used, isolated yields and  $K_i$  values. See Supplementary Information for additional details.



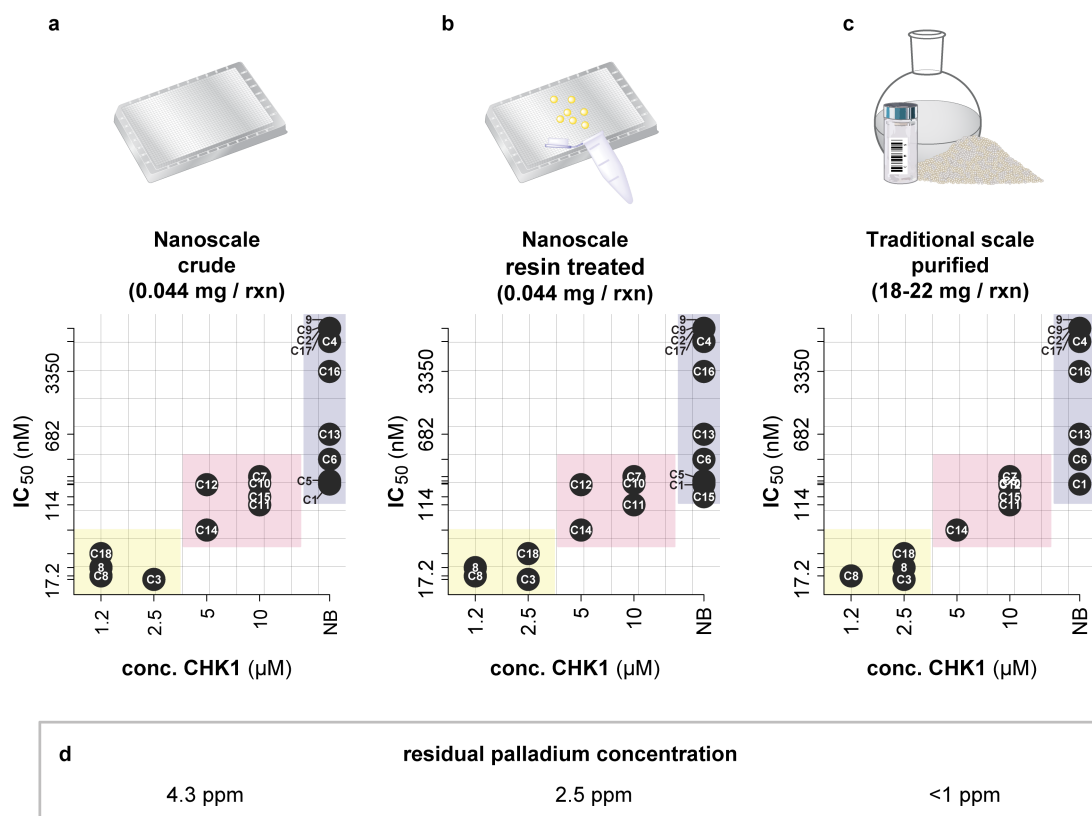
**Extended Data Fig. 3 | Structures, yields,  $IC_{50}$  values and ASMS comparison plots for the MK2 Library.** **a**, A library of 18 unique MK2 inhibitors (5, 6, B1–B16) was produced by coupling 4 to diverse boronates

under eight reaction conditions (see Fig. 2b). **b–e**, As in Extended Data Fig. 2, but for MK2 and  $IC_{50}$  values instead of ERK2 and  $K_i$  values.



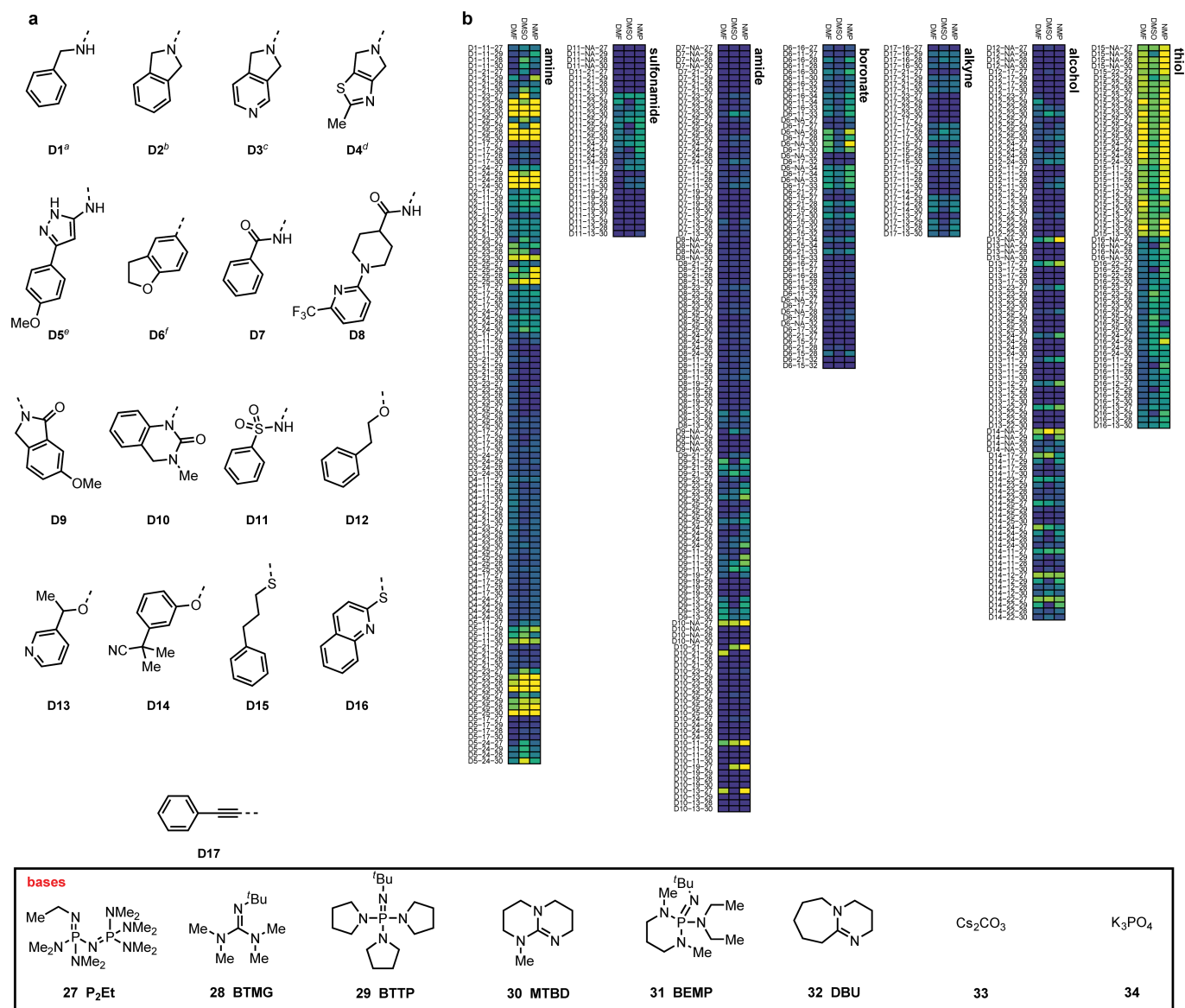
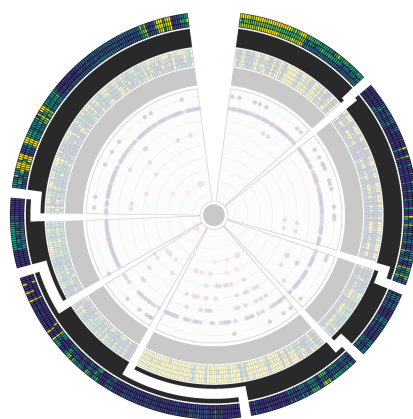
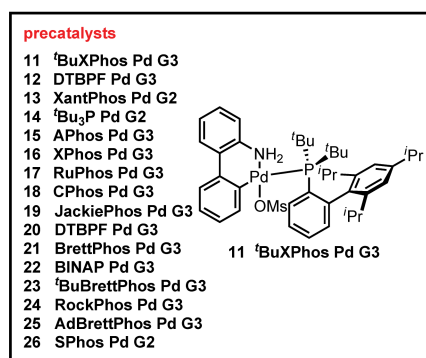
**Extended Data Fig. 4 | Structures, yields, IC<sub>50</sub> values and ASMS comparison plots for the CHK1 Library.** **a**, A library of 20 unique CHK1 inhibitors (8, 9, C1–C18) was produced by coupling 7 to diverse boronates

and amines under eight or nine reaction conditions (see Fig. 2c). **b–e**, As in Extended Data Fig. 2, but for CHK1 and IC<sub>50</sub> values instead of ERK2 and K<sub>i</sub> values.



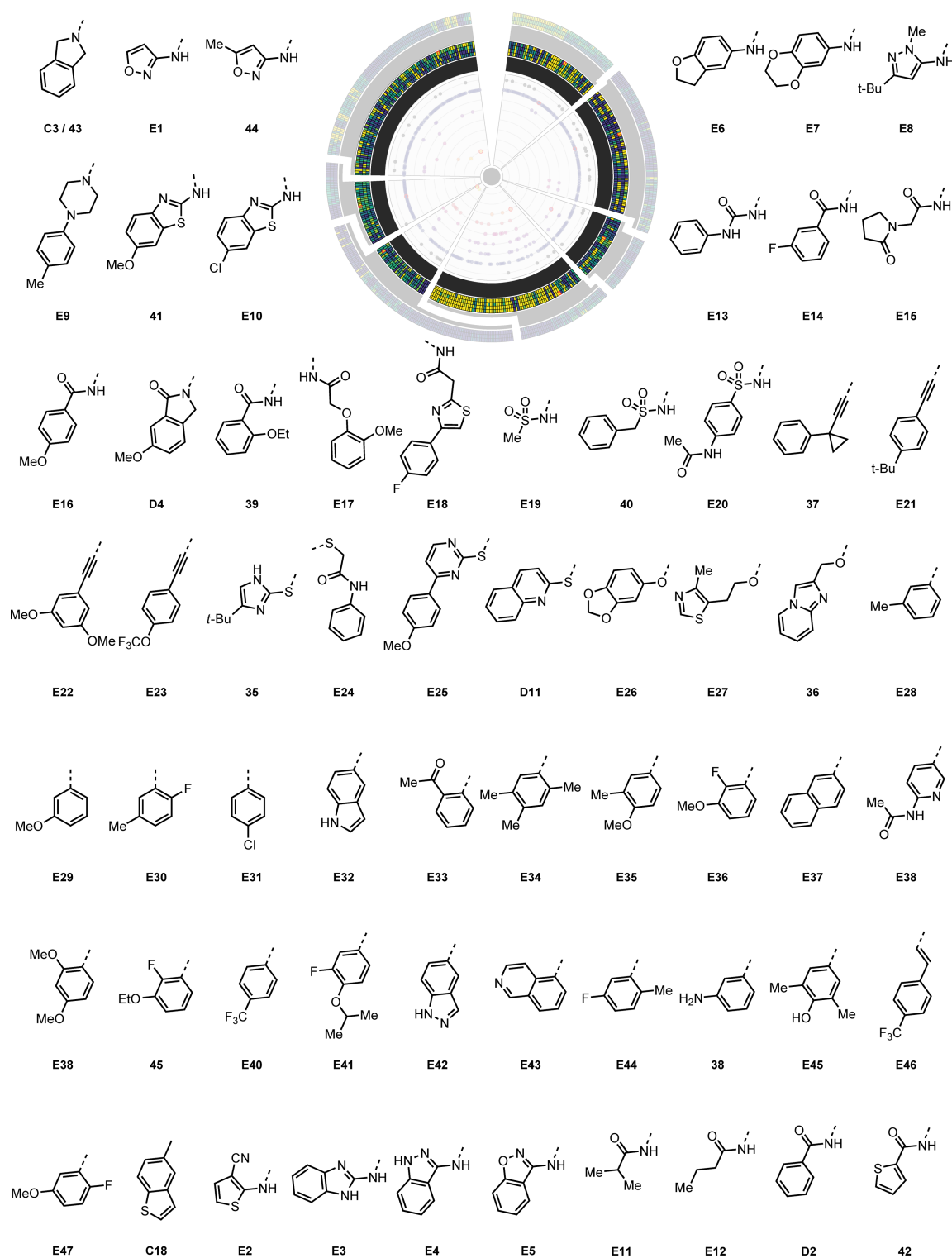
**Extended Data Fig. 5 | ASMS comparison plots for different reaction workup protocols and residual levels of palladium from the CHK1 library.** Reactions with different workup protocols were submitted to the ASMS assay, with affinity ranking determined by reducing the concentration of CHK1 to increase the competition for binding. The axes of the plots are as in Extended Data Fig. 4b, c. The reaction and workup protocols are as follows: **a**, nanoscale reactions submitted to

the affinity-ranking assay with no purification; **b**, nanoscale reactions submitted to the affinity-ranking assay following treatment with SiliaMets dimercaptotriazine (DMT) resin; and **c**, 50-mmol-scale reactions in which the product samples were purified by reverse-phase HPLC before submission to the affinity-ranking assay. See Supplementary Information for additional details.



**Extended Data Fig. 6 | Catalyst–base survey.** See Fig. 3. **a**, Diverse model nucleophiles (D1–D17) were screened against combinations of catalysts (11–26) and bases (27–34) in NMP, DMSO or DMF solvent. **b**, The details beside the heat maps show the mapping of nucleophiles, solvents, catalysts and bases. NA, no catalyst used. Reactions were run on a 100-nmol scale and analysed by UPLC–MS for conversion to products of the form of **10**

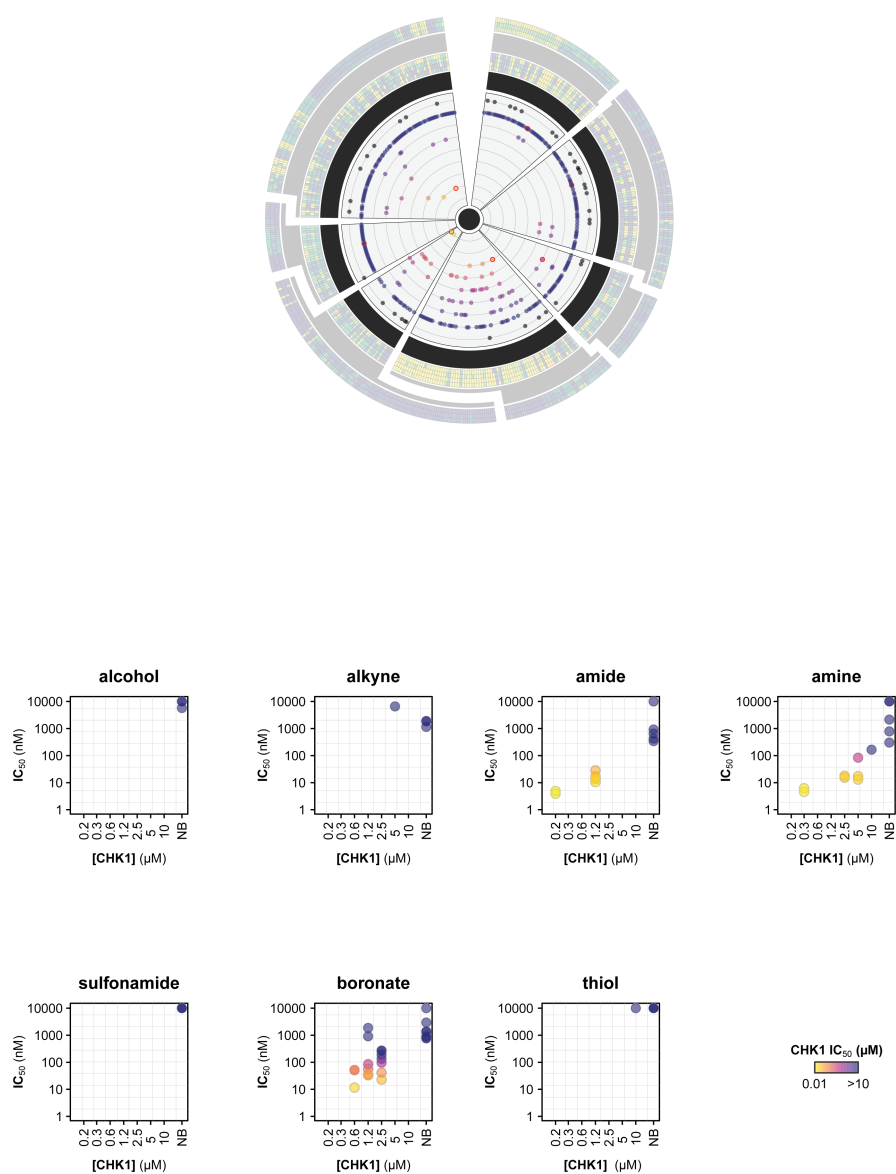
compared to a biphenyl internal standard. Productive reaction conditions from this screen were selected for use in the subsequent library synthesis campaign. <sup>a</sup>D1 is compound **C2** in Fig. 2c; <sup>b</sup>D2 is compound **C3** in Fig. 2c and **43** in Fig. 4; <sup>c</sup>D3 is compound **C5** in Fig. 2c; <sup>d</sup>D4 is compound **C6** in Fig. 2c; <sup>e</sup>D5 is compound **8** in Fig. 2c; <sup>f</sup>prepared from the boronic acid. See Supplementary Information for additional details.



322 additional nucleophiles were used generating 285 additional products.  
See Supporting Information.

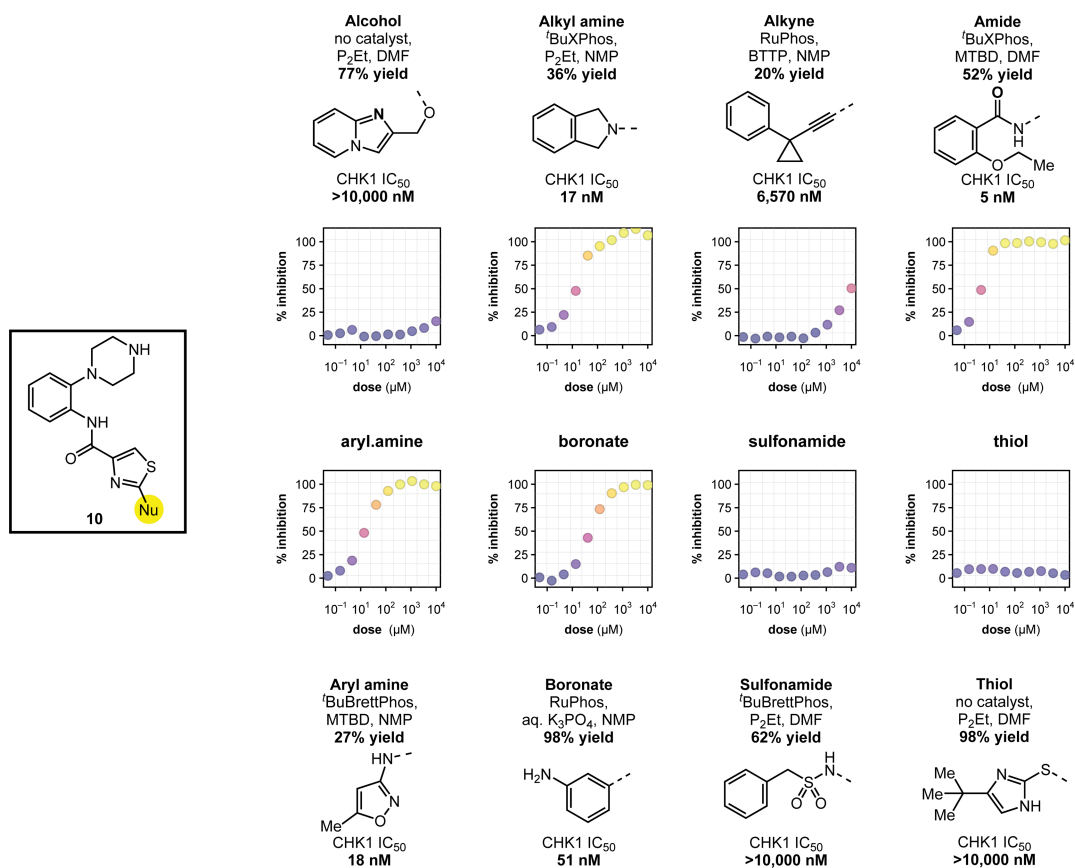
**Extended Data Fig. 7 | Exemplary compounds from the synthesis of the library.** See Fig. 3. Structures for 62 diverse coupling products (of the form of **10**) are shown, which were selected from the 345 productive reactions identified in a library synthesis campaign targeting 384 products

(Fig. 3). Diverse nucleophiles were coupled to **7** using the four reaction conditions selected in Fig. 3 and Extended Data Fig. 6. See Supplementary Information for additional details.



**Extended Data Fig. 8 | Comparison of the results of affinity ranking with  $IC_{50}$  values for inhibition of CHK1 functional activity.** The 62 exemplary compounds (Extended Data Fig. 6) were selected from 345 that were submitted to affinity ranking (Fig. 3). Crude nanoscale reactions were submitted to the ASMS assay, with affinity ranking determined

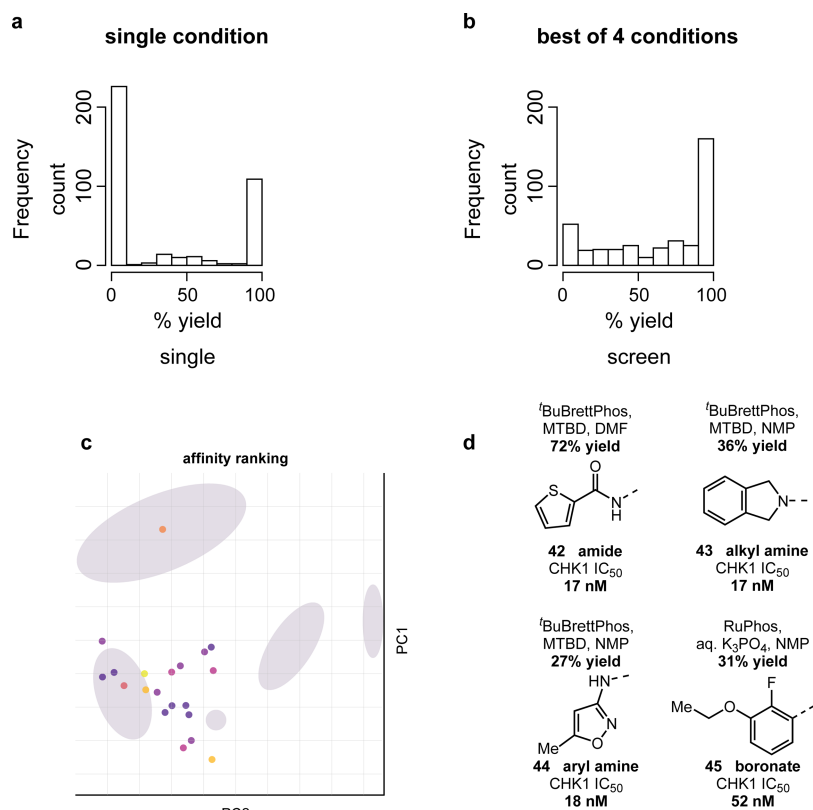
by reducing the concentration of CHK1 to increase the competition for binding. The axes of the plots are as in Extended Data Fig. 4b, c. Points are coloured by the  $IC_{50}$  value for inhibition of CHK1 function (as in Extended Data Fig. 4d). See Supplementary Information for additional details.



### Extended Data Fig. 9 | Dose response curves for exemplary compounds.

The compounds shown are 35–41 and 43. The inhibition of CHK1 functional activity by diverse coupling products (**10**) from the reaction of **7** with nucleophiles under various reaction conditions is shown. Isolated yields were achieved when the reaction conditions shown were

used. The dose response curves and IC<sub>50</sub> values shown were measured on purified product samples generated on a 50-μmol scale and could be predicted from affinity-ranking results of crude nanoscale reactions as shown in Extended Data Fig. 8. See Supplementary Information for dose response curves of additional compounds.



**Extended Data Fig. 10 | Reaction metrics and chemical ‘dark’ space.** **a**, Histogram of reaction performance for 384 diverse coupling reactions with bromide **7** using a single reaction condition (10 mol% <sup>t</sup>BuXPhos Pd G3, P2Et, NMP). Only 158 of the 384 targeted products were observed by mass spectrometry and the majority of the reactions failed (0% conversion to product). **b**, Histogram of reaction performance for 384 diverse coupling reactions with bromide **7** using the best of four reaction conditions, as described in Extended Data Figs. 6 and 7. Of the 384 targeted products, 345 were observed by mass spectrometry, with a more even distribution of reaction yields and the majority of reactions succeeding (100% conversion to product). **c**, Principal-component (PC) analysis of chemical ‘dark’ space, with each dot representing a compound

that was not formed under a single reaction condition (0% yield) but that had affinity to CHK1. By using the best of four reaction conditions, 187 additional products were produced and assayed that bound to CHK1; the colour of the dots reflects the affinity ranking of the compounds. The boundaries of this space are identical to those depicted in Fig. 4a, in which purple shading highlights additional regions where the majority of reactions failed (0% yield). Areas where dots are shown in purple shaded regions depict products with affinity to CHK1 that were formed in 0% yield in **a** but in more than 1% yield in **b**. **d**, Potent CHK1 inhibitors that were produced in 0% yield under a single condition (10 mol% <sup>t</sup>BuXPhos Pd G3, P2Et, NMP), but in modest to good yields following reaction-condition screening.